# Internal plasma potential measurements of a Hall thruster using plasma lens focusing

Jesse A. Linnell[a] and Alec D. Gallimore
*Plasmadynamics and Electric Propulsion Laboratory, Department of Aerospace Engineering,*
*University of Michigan, 1919 Green Road, Room B107, Ann Arbor, Michigan 48109*

Magnetic field topology has been found to be a central design concern for high-efficiency Hall thrusters. For future improvements in Hall thruster design, it is necessary to better understand the effects that magnetic field topology has on the internal plasma structure. The Plasmadynamics and Electric Propulsion Laboratory's High-speed Axial Reciprocating Probe system is used in conjunction with a floating emissive probe to map the internal plasma potential structure of the NASA-173Mv1 Hall thruster [R. R. Hofer, R. S. Jankovsky, and A. D. Gallimore, J. Propul. Power **22**, 721 (2006); **22**, 732 (2006)]. Measurements are taken at 300 and 500 V with a xenon propellant. Electron temperature and electric field are also measured and reported. The acceleration zone and equipotential lines are found to be strongly linked to the magnetic field lines. Moreover, in some cases the ions are accelerated strongly toward the center of the discharge channel. The agreement between magnetic field lines and equipotential lines is best for high-voltage operation. These results have strong implications on the performance and lifetime optimization of Hall thrusters. © *2006 American Institute of Physics*. [DOI: 10.1063/1.2358331]

## I. INTRODUCTION

Hall thrusters are space propulsion devices that use crossed electric and magnetic fields to ionize and accelerate propellant atoms to high exhaust velocities. The applied magnetic field impedes the motion of electrons resulting in the creation of a self-consistent electric field. The magnetic field has been shown to have a strong effect on the overall Hall thruster efficiency.[1–5] The focus of this research is to study the effect that magnetic field topology has on the internal plasma potential structure of Hall thrusters.

An important magnetic field topological feature in any state-of-the-art Hall thruster is what is commonly referred to as a plasma lens.[1,2,6–9] A plasma lens uses curved magnetic field lines that create electric fields that focus ions toward the center of the discharge channel. This phenomena can be explained because, to first order, the magnetic field lines chart the equipotential lines inside a Hall thruster.[8,10] The NASA-173Mv1 Hall thruster utilizes a plasma lens topology, which has been shown to improve beam focusing, ion acceleration processes, and internal electron dynamics.[2–5] Notable investigations of the internal plasma properties by Bishaev and Kim[11] and Haas[12] show at best a weak correlation between the magnetic field lines and the equipotential lines. However, with improvements in thruster design in the past years, the reexamination of the internal Hall thruster phenomena is a worthy pursuit.

This research employs a floating emissive probe that is swept at high speed into the Hall thruster discharge channel to map the internal plasma structure. Previous work has used similar methods to characterize the internal potential structure of Hall thrusters.[12–16] Haas[12] also mapped the entire discharge channel of the UM/AFRL P5 with this technique, which he pioneered. Haas noticed strong defocusing equipotential lines in the P5 at a discharge voltage and current of 300 V and 10 A, respectively. Keidar[17] shows that this behavior is related to a change in the electron mobility due to the magnetic field gradient and due to a radial electron temperature gradient.

A plasma lens magnetic topology leads to an additional effect of creating a magnetic mirror. A magnetic mirror results in a magnetic field magnitude near the discharge channel walls which is large in comparison to the channel centerline. This creates a force that acts to focus the electrons toward the center of the discharge channel. Keidar studied the effect of a magnetic mirror on potential structures inside the discharge channel.[18] In traditional thinking, the thermalized potential should match the magnetic field lines. Keidar shows that a radial magnetic field gradient may result in deviation between the electric potential and the thermalized potential, which acts to increase the potential in regions of high magnetic field. Furthermore, this study showed that a focusing potential structure could be obtained even in regions with primarily radial magnetic fields.

The present work is unique in that the NASA-173Mv1 has a vastly different magnetic field topology than the UM/AFRL P5. Unfortunately, the design of the NASA-173Mv1 is restricted under the International Traffic in Arms Regulation (ITAR). For this reason, only limited details on the thruster design are given.

## II. EXPERIMENTAL SETUP AND APPARATUS

### A. Experimental setup

The measurements reported in this paper were conducted in the Large Vacuum Test Facility (LVTF) at PEPL. The LVTF is a cylindrical stainless-steel tank that is 9 m long and

---
[a]Electronic mail: jlinnell@umich.edu
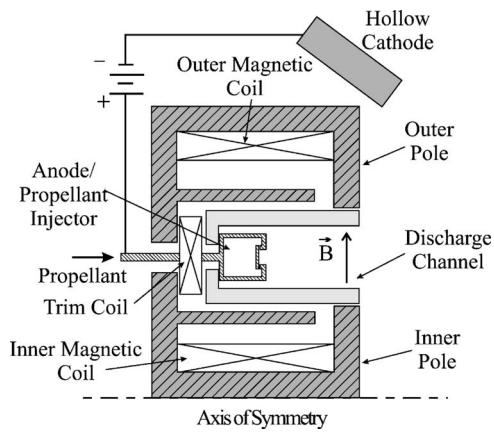
     **13**, 103504-1     

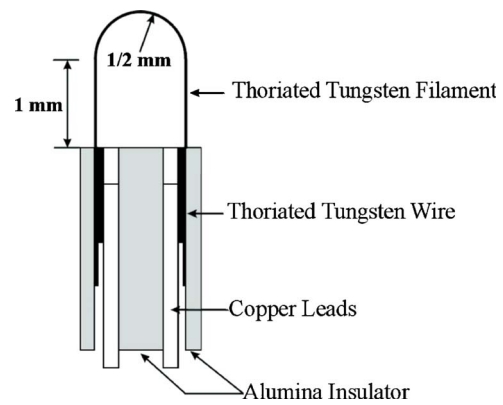FIG. 1. Generalized schematic of the magnetic circuit.



FIG. 2. Emissive probe schematic.

6 m in diameter. The vacuum chamber operates at a base pressure of $1.5 \times 10^{-7}$ Torr and approximately $3.3 \times 10^{-6}$ Torr during all thruster operating points.

The NASA-173Mv1 Hall thruster[2,4,5] is used for all measurements. The NASA-173Mv1 is mounted on two linear (radial and axial) tables that control the probe alignment and positioning. A generalized schematic of the NASA-173Mv1 magnetic circuit appears in Fig. 1. In addition to the standard inner and outer magnetic coils, the NASA-173Mv1 uses a trim coil to shape the magnetic field topology. Because of its location behind the anode, the trim coil modifies the radial magnetic field in the rear of the discharge channel. By using a negative coil current, the trim coil produces a negative magnetic field that increases the electrostatic plasma lens and the axial gradient of the radial magnetic field. Additionally, the trim coil creates a magnetic mirroring effect. This magnetic field topology results in the focusing of electrons and ions toward the center of the discharge channel.[19,20] The thruster is operated for 1 h for initial conditioning and is warmed up for at least 30 min at a given operation point before data are taken. A Busek BHC-50-3UM hollow cathode is used for all measurements.

The emissive probe is mounted on the HARP system,[21,22] which is securely fixed downstream of the thruster to dampen any vibrations caused by the high acceleration of the probe. The HARP has a linear motor assembly providing direct linear motion at very high speed and large acceleration.

## B. Emissive probe

### 1. Probe description

The emissive probe is composed of a 1.5-mm-diam double bore alumina insulator. The emitting filament is 1% thoriated tungsten with a diameter of 0.0127 cm. The NASA-173Mv1 has a maximum magnetic field of approximately 250 G, resulting in an electron gyroradius inside the Hall thruster that is smaller than the diameter of the emitting filament. This condition is necessary for unmagnetized probe theory to be valid.[23] A schematic of the emissive probe design appears in Fig. 2.

The area mapped by the emissive probes is displayed in Fig. 3. The origin is taken to be the location where the inner

wall meets the anode. Five axial sweeps spaced 5 mm apart are taken inside the Hall thruster discharge channel and data are shown for the region between 10 and 60 mm from the anode. The emissive probe is positioned so that the plane of the filament loop is normal to the thruster radial direction. The expected resolution of the emissive probe is 1.5 mm, which is the approximate size of the filament loop. For this experiment, the probe is swept at 150 cm/s and residence time inside the discharge channel is kept under 80 ms.

The floating emissive probe circuit consists of the emissive probe, an isolation amplifier, and a floating power supply capable of supplying enough current to heat the filament (3–4 A). The sampling rate is set to sample every 0.5 mm, which results in aliasing of the signal so that high frequency oscillations cannot be resolved. Therefore, these data are considered "time-averaged" measurements. The perturbations to the discharge current and cathode potential are also recorded. During post processing, a gentle spline smoothing is used to reduce the signal noise from the probe position, and floating probe potential. Examples of a typical data sweep are given in Fig. 4, which shows the floating potential and the perturbations to the thruster as the probe is swept into the discharge channel. In this figure $V_p$ is the plasma potential, $V_k$ is the cathode potential, and $I_D$ is the discharge current. For these reported data, the perturbations to the discharge current are below 15%–20%.
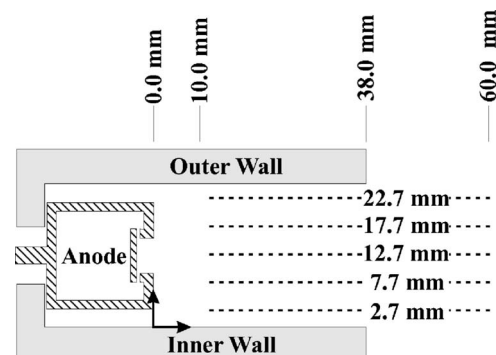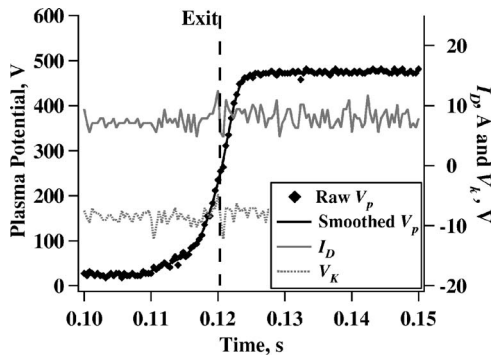


FIG. 3. Emissive probe mapping region.

FIG. 4. Emissive probe sweep example.

### 2. Space-charge-limited sheath correction

Space-charge effects must be taken into account when analyzing emissive probe data in Hall thrusters. The space-charge limit is reached when the emitted electron current to collected electron current ratio reaches a critical value approximately equal to 1.[24] Above this critical ratio, a potential well forms and emitted electrons are returned to the probe, creating a double sheath.

In order to correct for the space-charge-limited sheath, the measured plasma potential is augmented by adding the potential drop across the collector sheath $(0.6T_e)$.[19,24,25] This correction approach yields the instantaneous plasma potential local to the emissive probe while avoiding added complication from trying to correct for the large presheath. The collector sheath size $[\sim O(\lambda_D)]$ internal to the Hall thruster is on the same order as the wire diameter, which is an order of magnitude smaller than the total emitting tip dimensions. Therefore, the desired resolution of approximately 1.5 mm is maintained. Because of the presheath size is on the same order as the discharge channel width,[26] it is difficult to account for the presheath potential drop while maintaining a meaningful spatial resolution. The potential drop $(0.9T_e)$[25] across the presheath is considered a perturbation to the plasma and is used to define error bars for the measurement. In addition to the presheath perturbation, one half of the potential drop across the floating heater power supply should also be included as uncertainty. The heater filament potential drop is 4 V. Therefore, total error associated with the plasma potential measurements is equal to $\pm 0.9T_e$-2 V.

### 3. Electron temperature and electric field calculation

Electron temperature can be calculated by using both "hot" and "cold" probe measurements.[14] Cold measurements refer to measurements taken with no filament heating. Equation (1) uses the potential drop across the collector sheath and presheath to calculate the electron temperature. In this equation, $k_B$ is the Boltzmann constant, $T_e$ is the electron temperature, $V_f$ is the cold probe floating potential, and $e$ is the electron charge. The error in the temperature calculation is estimated to be $-17/+38\%$:[14]

$$V_p - V_f = -\frac{k_B T_e}{e}\ln\left(0.61\sqrt{\frac{2\pi m_e}{M_i}}\right). \tag{1}$$

Axial and radial electric fields at each location inside the thruster are also presented below. A central difference method is used with the plasma potentials to calculate the electric field. The forward difference technique is used for the first point, and backward difference approach for the last point.

## III. RESULTS AND DISCUSSION

The internal plasma potential is mapped for four operation points (see Table I). Data are taken at discharge voltages of 300 and 500 V, an anode flow rate of 10 mg/s, and with and without trim coil operation. For each operation point, performance was optimized by monitoring thrust and thruster operating conditions to calculate real time efficiencies, and adjusting the magnet coil currents accordingly.

For each operating condition the corrected plasma potential, electron temperature, axial electric field, and radial electric field are mapped. In each map, the magnetic field topology pathlines are overlaid with the plasma properties. The magnetic fields have been calculated using the three-dimensional (3D) magnetostatic solver Magnet 6.0 by Infolytica. Line plots for plasma potential, electron temperature, and axial electric fields are given along the discharge channel centerline for each operating condition.

From these plasma potential data, the start and end of the acceleration zone are determined by the location of the 10% and 90% potential drops between the near anode and downstream region. Although these criteria for determining the location of the acceleration zone is somewhat arbitrary, it was chosen to avoid error that could be introduced due to observer subjectivity. It seems logical that a better indicator of the boarders of the acceleration zone might be the magnitude of the axial electric field, unfortunately due to the noisiness of the electric field measurements, this can be very difficult. The average start, end, and length of the acceleration region, and the percentage of ion acceleration outside the discharge channel are given in Table II. It can be seen that

TABLE I. Operation points for internal plasma potential mapping.

| Point No. | $V_k$ (V) | $V_d$ (V) | $I_d$ (A) | Discharge power (W) | Anode flow (mg/s) | Cathode flow (mg/s) | IC current (A) | OC current (A) | TC current (A) | Thrust (mN) | Anode efficiency (%) |
|---|---|---|---|---|---|---|---|---|---|---|---|
| 1 | −10.5 | 300 | 9.17 | 2751 | 10.00 | 1.00 | 1.89 | 2.21 | 0.00 | 179 | 57.9 |
| 2 | −10.9 | 300 | 8.95 | 2684 | 10.00 | 1.00 | 1.88 | 2.21 | −0.51 | 180 | 61.2 |
| 3 | −11.5 | 500 | 9.35 | 4675 | 10.00 | 1.00 | 2.90 | 2.67 | 0.00 | 243 | 61.6 |
| 4 | −11.7 | 500 | 9.27 | 4635 | 10.00 | 1.00 | 2.90 | 2.87 | −0.87 | 247 | 66.1 |

TABLE II. Acceleration zone dimensions.

| Point No. | $V_d$ (V) | Trim coil? | Average length (mm) | Average start (mm) | Average end (mm) | Voltage drop outside (%) |
|---|---|---|---|---|---|---|
| 1 | 300 | No | 16.7 | 37.0 | 53.8 | 80.8 |
| 2 | 300 | Yes | 15.8 | 32.3 | 48.1 | 59.5 |
| 3 | 500 | No | 17.2 | 32.2 | 49.4 | 42.7 |
| 4 | 500 | Yes | 17.3 | 33.8 | 51.2 | 51.7 |

the start of the acceleration zone is very similar for all but the 300-V, no trim coil case. The acceleration length increases slightly with increased discharge voltage. The trim coil gives no conclusive trends as to the acceleration length and location. For all cases, a significant portion of the ion acceleration occurs outside of the discharge channel. It is likely that the location of the acceleration zone is dependent on the axial variation of the electron mobility.

### A. 300-V cases

#### 1. Haas's UM/AFRL P5 mapping

Internal emissive results from Haas[12] for the UM/AFRL P5 Hall thruster operation at 10 A and 300 V are shown in Fig. 5. Haas observed a strong defocusing of the equipotential lines. This behavior is also computationally confirmed by Keidar.[17] Both the UM/AFRL P5 and the NASA-173Mv1 have the same discharge channel dimensions. A comparison between these thrusters is important because it shows the effect that a different magnetic field topology has on thrusters with similar discharge channel dimensions and operating conditions.

#### 2. NASA-173Mv1 mapping

When the trim coil is energized, the thrust increases by 1 mN and the discharge current decreases by 0.22 A. This suggests a decrease in the electron current to the anode. The internal mappings for the 300-V cases with and without the trim coil are shown in Figs. 6–9. The case without the trim coil shows a slight defocusing of the equipotential lines downstream of the acceleration region and a focusing in the main acceleration region. The slight asymmetry in the acceleration zone can be explained by the asymmetry in the mag-
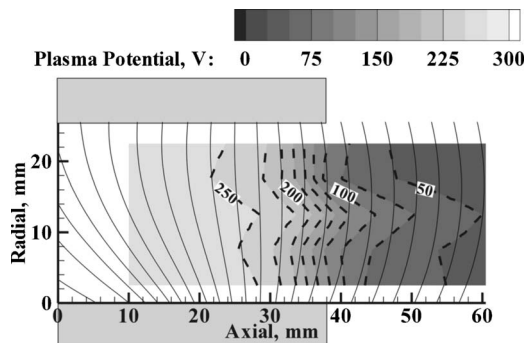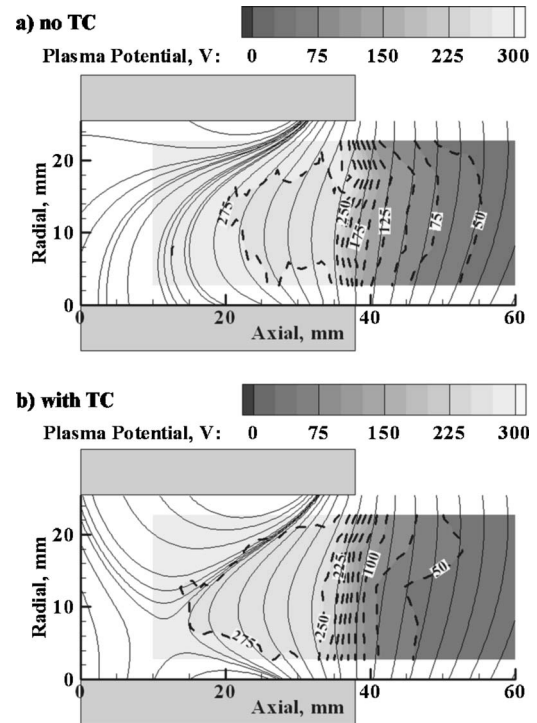


FIG. 6. Plasma potential map for the 300-V cases (a) without and (b) with the trim coil.

netic field lines. The trim coil case shows greater equipotential focusing in the regions upstream and downstream of the acceleration zone. This result can be explained by the stronger plasma lens focusing of the trim coil. The agreement between the equipotential lines and magnetic field lines is



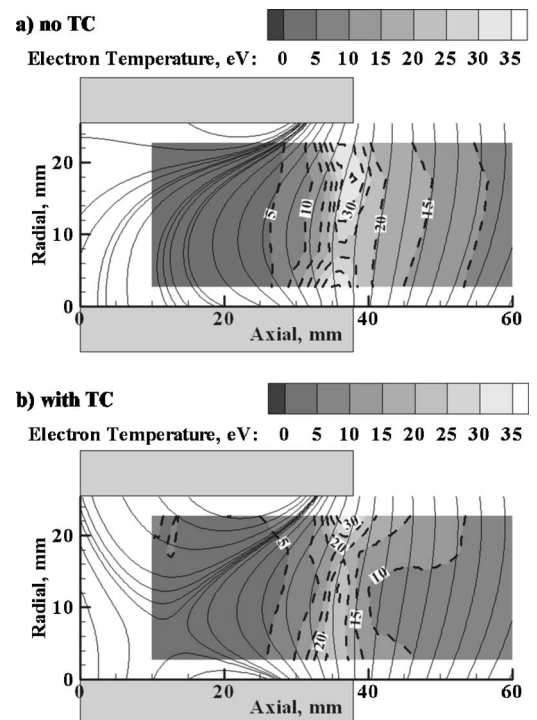FIG. 5. Plasma potential map for the UM/AFRL P5 Hall thruster operation at 10 A and 300 V (Ref. 12).



FIG. 7. Electron temperature map for the 300-V cases (a) without and (b) with the trim coil.
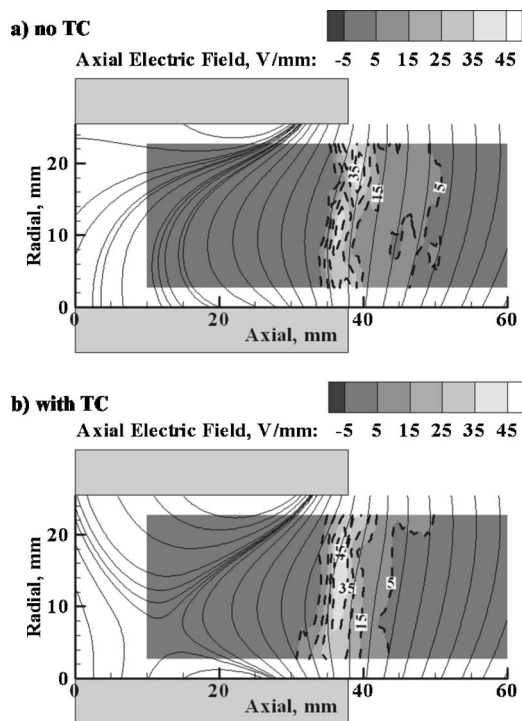
FIG. 8. Axial electric field for the 300-V cases (a) without and (b) with the trim coil.

not as strong in the acceleration zone due to the high electron temperature. This focusing behavior has also been predicted by Keidar[18] for a thruster using a magnetic mirror.

The location of maximum electron temperature begins just upstream and continues to the center of the acceleration
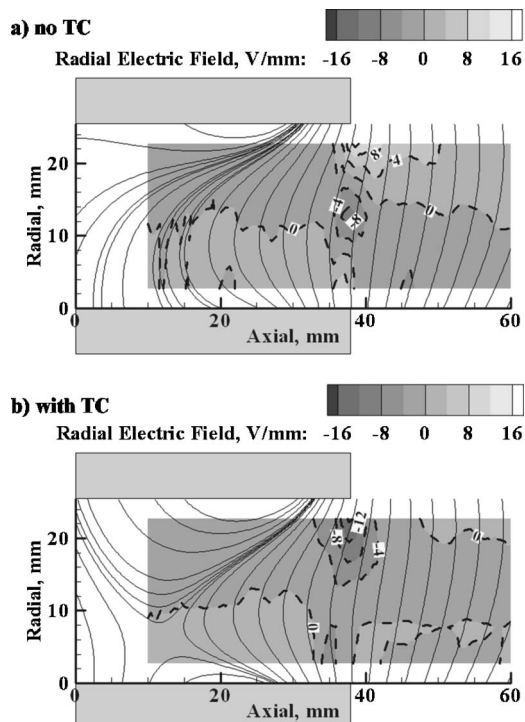


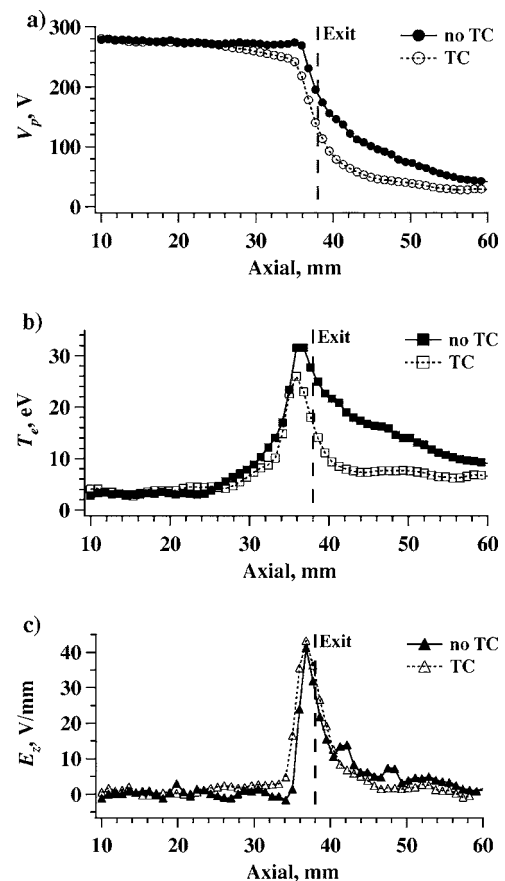FIG. 9. Radial electric field map for the 300-V cases (a) without and (b) with the trim coil.



FIG. 10. Centerline plasma properties for the 300-V non-trim coil and trim coil conditions.

zone for both the case with and without the trim coil. The maximum electron temperature is approximately 35 eV for the case without the trim coil. For the trim coil case, the electron temperature reaches a maximum of approximately 27 eV for most of the discharge channel, although it does reach an electron temperature of 34 eV on the outer wall. Both 300-V cases have a maximum axial electric field of approximately 45 V/mm.

Centerline plasma properties are shown in Fig. 10. The acceleration zone is located further upstream for the 300-V trim coil case. For the trim coil case there is a slow decrease in plasma potential between 26 and 35 mm. This slow decrease then transitions into the rapid decline in plasma potential that is similar to the non-trim coil case. This slow decrease is unusual and not well understood, however the trim coil case does not have a larger magnetic field than the non-trim coil case.

The acceleration region plots for the 300-V settings are given in Fig. 11. Although the finer details of the acceleration zone structure are lost on this plot, it is still possible to see the defocusing plasma potential structure in the non-trim coil case and the focusing plasma structure in the trim coil case. Figure 11 shows that a large percentage of the ion acceleration occurs outside of the discharge channel.
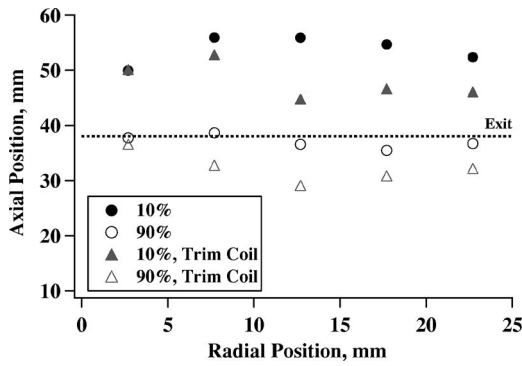
FIG. 11. Acceleration region boundaries for the 300-V cases.

## B. 500-V cases

The internal emissive probe mappings for the 500-V cases with and without the trim coil are given in Figs. 12–15. The use of the trim coil results in an increase in thrust of 5 mN or 1.6% and a decrease in discharge current of 0.08 A. The increase in thrust is likely due to the improvement in beam focusing. These cases show a remarkable correlation between the focusing magnetic field lines and the plasma potential. The non-trim coil case has an equipotential asymmetry that can be explained by an asymmetry in the magnetic field lines. The trim coil case has a strong focusing in the equipotential lines that is due to the focusing effect of the magnetic lens. Even the defocusing magnetic field lines downstream of the discharge channel correspond to defocusing equipotential lines. The ion focusing is clearly shown by the radial electric fields in Fig. 15. The radial electric fields focus the ions into the center of the discharge channel and
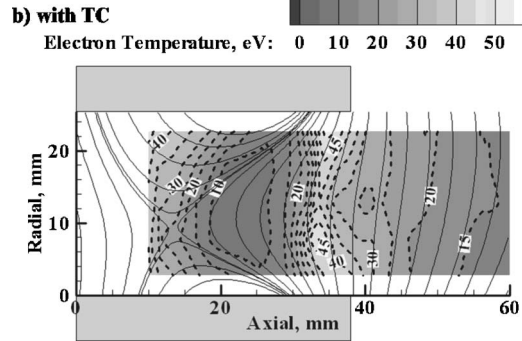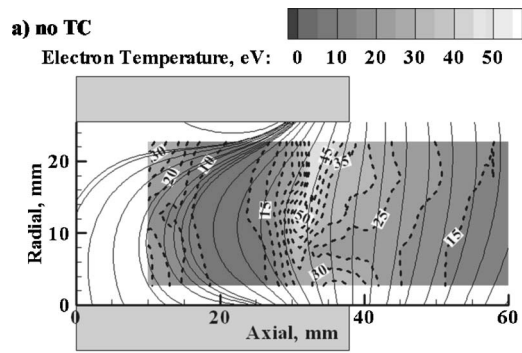


FIG. 13. Electron temperature map for the 500-V cases (a) without and (b) with the trim coil.

are approximately 12–18 V/mm while the axial electric field reaches a maximum of about 70 V/mm in the trim coil case. Similarly, the axial electric field reaches a maximum of approximately 80 V/mm in the non-trim coil case.

A possible explanation of the improved ion focusing at higher voltage is due to electron temperature saturation.
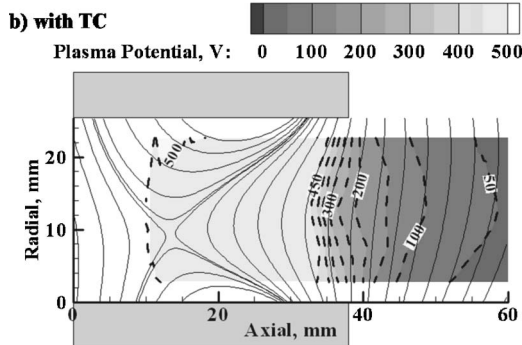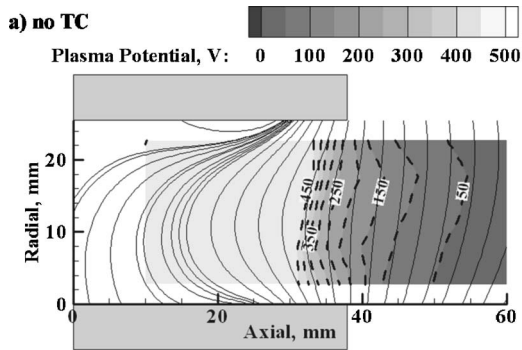


FIG. 12. Plasma potential map for the 500-V cases (a) without and (b) with the trim coil.
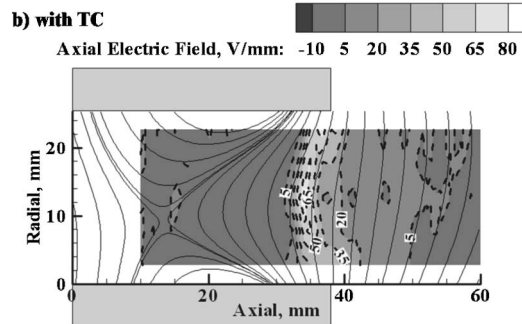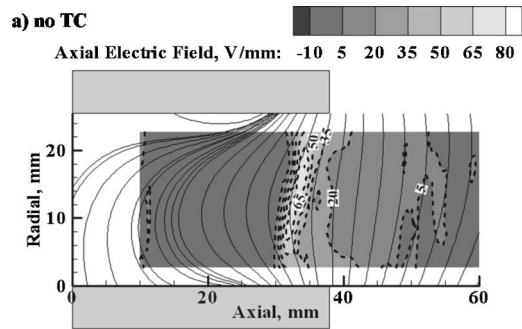


FIG. 14. Axial electric field map for the 500-V cases (a) without and (b) with the trim coil.
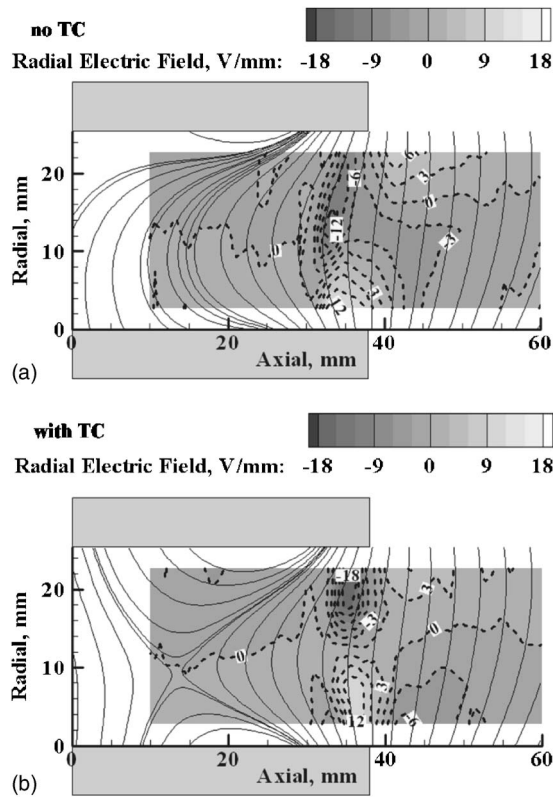
FIG. 15. Radial electric field map for the 500-V cases (a) without and (b) with the trim coil.



FIG. 16. Centerline plasma properties for the 500-V non-trim coil and trim coil conditions.

Electron temperature saturation is a behavior that has been both predicted computationally[27,28] and observed experimentally.[14,15] Since thermalized potential follows the magnetic field lines, the equipotential lines should differ from the magnetic field line by roughly the electron temperature. As discharge voltage increases past 400 V, the electron temperature is shown to saturate to 50–60 eV.[14,15] This saturation results in a greater ratio of plasma potential to electron temperature and the equipotential lines follow the magnetic field lines more closely. This larger plasma potential to electron temperature ratio is shown by Langmuir probe measurements for these operation conditions.[20] The Langmuir probe results show a maximum electron temperature for the 300 and 500-V trim coil cases of 40 and 50 eV, respectively. The electron temperature measurements from the Langmuir probe results are expected to be more accurate than the emissive probe measurements. Consistent with this observed trend, in the Bishaev and Kim[11] experiment where they observed weak correlation between equipotential lines and magnetic field lines, the thruster was operated at a discharge voltage of only 200 V. Unfortunately, this explanation is conjecture and additional measurements over a large range of discharge voltages are necessary to confirm this theory.

Similar to the 300-V cases, both 500-V cases show a region of high electron temperature immediately upstream of the acceleration zone that continues into the acceleration zone. The electron temperature of both trim coil and non-trim coil cases reaches a maximum of 45–50 eV. As a result of increased Joule heating,[14,15,27,28] the electron temperature is higher for the 500-V cases than the 300-V cases
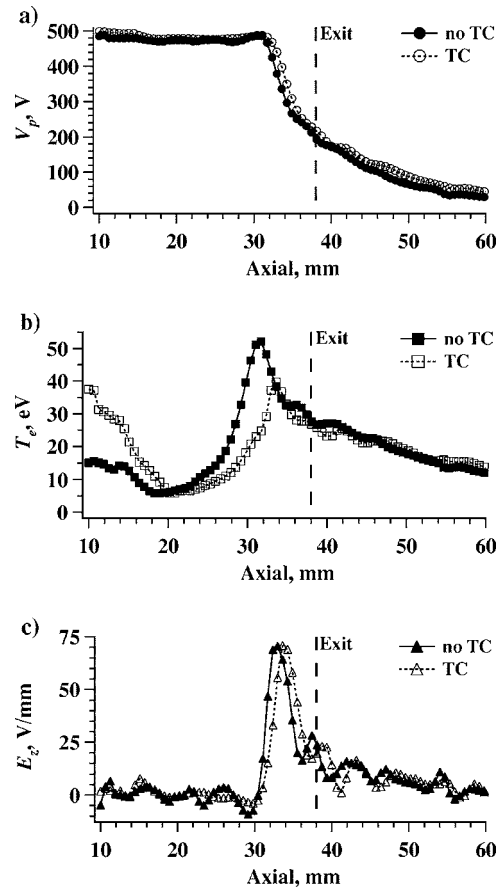
(27–35 eV). The higher voltage operation points also display an additional region of increased electron temperature near the anode that is comparable to the "hot" region near the acceleration zone.

This near-anode hot zone is unusual although a similar trend is observed by Meezan *et al.*[13] Internal Langmuir probe measurements show that this near-anode hot zone probably does not exist and may be an artifact of the floating emissive probe technique for calculating the electron temperature.[20] The cold probe measurements used to calculate the electron temperature [Eq. (1)] measured an artificial drop in floating potential not observed in the Langmuir probe data. The source of this near-anode hot zone is not entirely clear, although the magnetic field can cause a significant change on the probe collection area and the electron dynamics near the probe. The near-anode hot zone is extremely well correlated with a decrease in the radial component in the magnetic field and with magnetic field lines that are predominantly axial. When the radial component approaches zero Gauss, the electron current appears to be enhanced resulting in a decreased floating potential measurement. However, this error in electron temperature is only a concern near the anode and the electron temperatures elsewhere in the discharge channel are considered more reliable.

Centerline plasma properties are shown in Fig. 16 and the acceleration zone boundaries for the 500-V case can be seen in Fig. 17. These plots show that the location of accel-
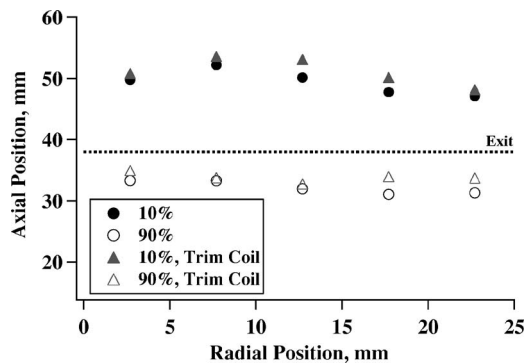
FIG. 17. Acceleration region boundaries for the 500-V cases.

eration zone for the trim coil and non-trim coil cases are very similar and that the trim coil has little effect on the acceleration zone.

### C. Thermalized potential

Morozov[8] first suggested that to the first order, the magnetic field lines should predict the equipotential lines inside the Hall thruster. More accurately, assuming that the electron pressure is negligible, the thermalized potential should follow the magnetic field lines. The thermalized potential is given by $V_p^* = V_p + T_e \ln(n_e/n_o)$. In this equation $n_e$ is the electron number density, $n_o$ is a reference number density set equal to $1 \times 10^{12}$ cm$^{-3}$, and $T_e$ is given in units of eV. For completeness, the thermalized potential is calculated for the 300-V and 500-V cases both with the trim coil are shown in Fig. 18. The electron temperature and plasma number density (assuming quasineutrality) are taken from internal Langmuir
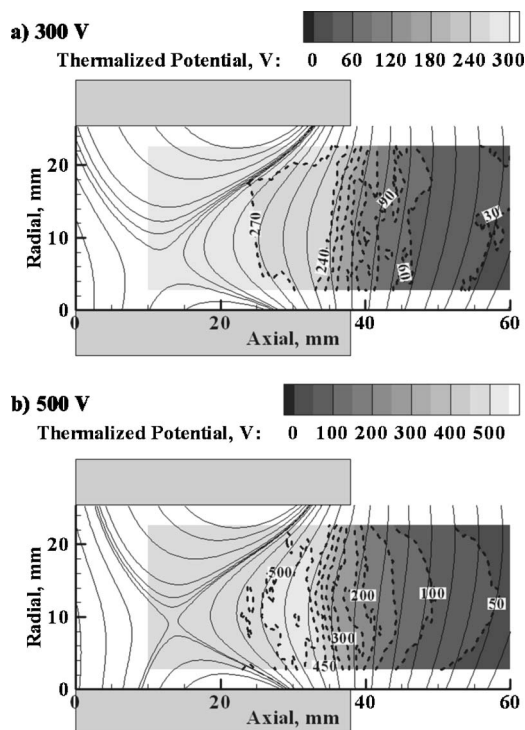
probe measurements for these operating condition.[20] Although further comparison between the emissive probe and Langmuir probe results are out of the scope of this article, it should be noted that in Fig. 18 the electron temperature measured from the Langmuir probe is used for the emissive probe correction. Given the error associated with any probe measurement, the thermalized potential correlation with the magnetic field lines shows good agreement everywhere in the mapped region.

## IV. CONCLUSIONS

The internal plasma structure inside the NASA-173Mv1 has been successfully mapped. The equipotential lines are shown to follow the magnetic field lines everywhere although to a lesser degree in the high-electron temperature region of the acceleration zone. However, for high-voltage operation, the magnetic field lines are shown to be well correlated with the equipotential lines in the entire discharge channel. In the 500-V, trim coil case, the ions are shown to be strongly accelerated toward the center of the discharge channel. This effect has strong implications for future Hall thruster designs and thruster life.

The trim coil is shown to improve the ion focusing by increasing the plasma lens. Radial electric fields are often greater than 20% of maximum axial electric field. The trim coil may have a small effect on the acceleration zone location or length although more data are necessary before a conclusion can be made. The trim coil is found to have little effect on electron temperature. Maximum electron temperature increases with discharge voltage, and reaches approximately 27–35 and 45–50 eV for the 300-V and 500-V cases, respectively.

FIG. 18. Thermalized potential map for the (a) 300-V and (b) 500-V trim coil cases.

[1] R. R. Hofer and A. D. Gallimore, *Proceedings of the 38th AIAA/ASME/SAE/ASEE Joint Propulsion Conference*, Indianapolis, IN, 7–10 July 2002 (American Institute of Aeronautics and Astronautics, Reston, VA, 2002), AIAA-2002–4111.

[2] R. R. Hofer, Doctoral thesis, University of Michigan, 2004.

[3] J. A. Linnell and A. D. Gallimore, "Efficiency analysis of a Hall thruster operating with krypton and xenon," J. Propul. Power (to be published).

[4] R. R. Hofer, R. S. Jankovsky, and A. D. Gallimore, J. Propul. Power **22**, 721 (2006).

[5] R. R. Hofer, R. S. Jankovsky, and A. D. Gallimore, J. Propul. Power **22**, 732 (2006).

[6] V. Kim, J. Propul. Power **14**, 736 (1998).

[7] V. M. Gavryshin, V. Kim, V. I. Kozlov, and N. A. Maslennikov, *Proceedings of the 24th International Electric Propulsion Conference*, Moscow, Russia, 19–23 September 1995 (Electric Rocket Propulsion Society, Cleveland, OH, 1995), IEPC-1995-038.

[8] A. I. Morozov, Sov. Phys. Dokl. **10**, 775 (1966).

[9] A. I. Bugrova, A. I. Morozov, G. B. Popkov, and V. K. Kharchevnikov, Sov. Phys. Tech. Phys. **31**, 2 (1986).

[10] A. I. Morozov, Y. V. Esinchuk, G. N. Tilinin, A. V. Trofimov, Y. A. Sharov, and G. Y. Shchepkin, Sov. Phys. Tech. Phys. **17**, 38 (1972).

[11] A. M. Bishaev and V. Kim, Sov. Phys. Tech. Phys. **23**, 1055 (1978).

[12] J. M. Haas and A. D. Gallimore, Phys. Plasmas **8**, 652 (2001).

[13] N. B. Meezan, W. A. Hargus, and M. A. Cappelli, Phys. Rev. E **63**, 026410 (2001).

[14] Y. Raitses, D. Staack, A. Smirnov, and N. J. Fisch, Phys. Plasmas **12**, 073507 (2005).

[15] Y. Raitses, D. Staack, M. Keidar, and N. J. Fisch, Phys. Plasmas **12**, 057104 (2005).

[16] D. Staack, Y. Raitses, and N. J. Fisch, Appl. Phys. Lett. **84**, 3028 (2004).

[17] M. Keidar, A. D. Gallimore, Y. Raitses, and I. D. Boyd, Appl. Phys. Lett. **85**, 2481 (2004).

[18] M. Keidar and I. D. Boyd, Appl. Phys. Lett. **87**, 121501 (2005).

[19] J. A. Linnell and A. D. Gallimore, *Proceedings of the 29th International Electric Propulsion Conference*, Princeton, NJ, 31 October– 4 November 2005 (Electric Rocket Propulsion Society, Cleveland, OH, 2005), IEPC-2005-024.

[20] J. A. Linnell and A. D. Gallimore, *Proceedings of the 42nd AIAA/ASME/ SAE/ASEE Joint Propulsion Conference*, Sacramento, CA, 9–12 July 2006 (American Institute of Aeronautics and Astronautics, Reston, VA, 2006), AIAA-2006-4470.

[21] J. M. Haas, "Low-perturbation interrogation of the internal and near-field plasma structure of a Hall thruster using a high-speed probe positioning system," Doctoral thesis, University of Michigan, 2001.

[22] J. M. Haas, A. D. Gallimore, K. McFall, and G. Spanjers, Rev. Sci. Instrum. **71**, 4131 (2000).

[23] N. Hershkowitz and M. H. Cho, J. Vac. Sci. Technol. A **6**, 2054 (1988).

[24] G. D. Hobbs and J. A. Wesson, Plasma Phys. **9**, 85 (1967).

[25] L. A. Schwager, Phys. Fluids B **5**, 631 (1993).

[26] M. Keidar, I. D. Boyd, and I. I. Beilis, Phys. Plasmas **8**, 5315 (2001).

[27] E. Ahedo and D. Escobar, J. Appl. Phys. **96**, 983 (2004).

[28] S. Barral, K. Makowski, Z. Peradzyski, N. Gascon, and M. Dudeck, Phys. Plasmas **10**, 4137 (2003).